Effect of a Micro-crack on the Edge Macro-crack Propagation Rate and Path Under Mixed Loads

Xiaotao Li[1]   Xiaoyu Jiang[1*]

([1] School of Mechanics and Engineering, Southwest Jiaotong University, No. 111, North 1st Section of Second
Ring Road, Jinniu District, Chengdu City 610031, Sichuan Province, China)

ABSTRACT The solution of a half-plane containing a micro-crack and an edge macro-crack under mixed loads is presented based on the distributed dislocation technique. The complete stress field and stress intensity factors are obtained. The finite element model is established to simulate the macro-crack propagation path. The effect of a micro-crack on the macro-crack propagation is analyzed comprehensively. The results show that the shielding effect region is like two 'petals' under uniaxial tensile load and rotates with the change in micro-crack angle. For mixed loads, the shielding effect region rotates clockwise with the increasing ratio of applied loads $\tau^\infty/\sigma^\infty$. It is like two 'petals' at $\tau^\infty/\sigma^\infty \leq 2$ and divides into two parts from the macro-crack tip at $\tau^\infty/\sigma^\infty \geq 5$. The micro-crack has the attraction effect on the macro-crack propagation path. These results are useful for predicting the fracture or fatigue behaviors of materials containing micro-cracks.

KEY WORDS Micro-crack, Macro-crack propagation, Distributed dislocation technique, Complete stress field

List of Symbols

a Half-length of the micro-crack
l Initial macro-crack length
θ Micro-crack orientation
α Micro-crack angle
d Distance between the macro-crack tip and the micro-crack center
σ^∞ Uniform tensile load
τ^∞ Uniform shear load
$\tilde{\sigma}_{ij}$ Stress components contributed by the applied loads
$\bar{\sigma}_{ij}$ Stress components contributed by distributed dislocations
x_{micro} Horizontal ordinate of the micro-crack center
y_{micro} Vertical ordinate of the micro-crack center
K_{eff} Equivalent stress intensity factor
K_{eff}^∞ Equivalent stress intensity factor for the case without micro-crack
K_{I}^∞ Mode I stress intensity factor for the case without micro-crack
K_{I} Mode I stress intensity factor at the macro-crack tip

---

* Corresponding author. E-mail: xiaoyujiang8@sohu.com; xiaoyujiang8@sina.com

K_{II} Mode II stress intensity factor at the macro-crack tip

b_x, b_y Components of Burgers vector

μ Shear modulus

κ Kolosov constant

$G(\xi, x, y)$ Dislocation influence function

$B(\xi)$ Dislocation density function

β Crack propagation direction

E Elasticity modulus

ν Poisson's ratio

σ_{von} von Mises stress

γ Intersection angle between the micro-crack face and the line composed by the micro-crack center and macro-crack tip

SIF   Stress intensity factor

ESIF   Equivalent stress intensity factor

FE   Finite element

FEM   Finite element method

DDT   Distributed dislocation technique

MCTSC   Maximum circumferential tensile stress criterion

1. Introduction

There are many micro-cracks in solid materials, which is very difficult to avoid. These micro-cracks have significant influences on the fatigue and fracture performances of materials. The formation of micro-cracks is random, so there is great uncertainty in fracture and fatigue tests. Fatigue and fracture are the most dangerous forms of materials' failure. Fracture mechanics has been studied widely since the last century. Fatigue and fracture behaviors can be predicted effectively by investigating the interaction between the micro-crack and macro-crack. In addition, the toughening effect of micro-cracks for brittle materials is an important research field. Therefore, the interaction problem between micro-cracks and a macro-crack has been considered by many researchers in recent decades.

Kachanov et al. [1–3] proposed a simple solution to solve crack problems and investigated the effect of multiple micro-cracks on a finite macro-crack. Based on the complex function method, Gong et al. [4–6] investigated the influence of a micro-crack on a semi-infinite macro-crack and analyzed the amplifying and shielding effects of the micro-crack on the macro-crack tip. Tamuzs and Petrova [7] considered the problem of two micro-cracks and a finite macro-crack in an infinite plane. Soh and Yang [8] investigated the effect of a cluster of micro-cracks on a macro-crack propagation by the FEM. Alam et al. [9] studied the influence of a crack on an edge crack propagation by experiments and simulations. Budyn et al. [10] studied the propagation paths of multiple cracks in an elastic media by the extended FEM. Bouiadjra et al. [11] investigated the effect of micro-cracks on the plastic zone by the FEM. Li et al. [12] studied the effect of a micro-crack on the SIF and plastic zone at a macro-crack tip in an infinite plane based on the DDT. The DDT is an effective tool to solve complex crack problems, which was introduced in detail by Hills et al. [13]. The basic idea of DDT is that cracks can be replaced equivalently by continuously distributed dislocations. Based on the DDT, Jin and Keer [14] analyzed the interactions between edge cracks in an elastic half-plane. The DDT was also applied to solve the problem of a finite plane containing cracks [15–18]. The interactions between cracks and inhomogeneities were also investigated in many studies based on the DDT [19–23]. Therefore, the DDT will be employed in this work.

There are two main aspects in the study of fracture mechanics: crack propagation direction and rate. The problem of crack propagation direction was investigated by many previous studies. Erdogan and Sih [24] proposed the MCTSC and verified the criterion by tensile fracture experiments. Palaniswamy and Knauss [25] proposed the maximum energy release rate criterion. Sih [26] proposed the minimum strain energy density criterion. Li [27] proposed the vector crack tip displacement criterion. Khan and Khraisheh [28] proposed the minimum plastic zone size criterion. Bouchard et al. [29], Dündar and Ayhan [30], Ayhan [31], Varfolomeev et al. [32] and Liu et al. [33] simulated the crack propagation path by the FEM. Considering the elastic solid, it is reasonable and convenient to predict the crack

propagation direction using the MCTSC, which, therefore, is applied in this study. The crack propagation rate is an important parameter for predicting the fatigue life of structures and materials. Many formulas were proposed to predict the crack propagation rate. The studies on crack propagation rate by Paris [34, 35], Elber [36], Newman [37] and Walker [38] showed a positive correlation between the crack propagation rate and the SIF. Therefore, in this paper, the SIF is applied to analyze the crack propagation rate qualitatively. In many cases, the material surface is a region of high stress or strain, so it is common for an edge crack to initiate at the material surface. The edge crack propagation has been an interesting problem and investigated by many researchers [9, 13, 14, 29, 39].

Few theoretical studies have been reported on the edge macro-crack propagation affected by a micro-crack in a half-plane. In this paper, the edge macro-crack propagation in the existence of a micro-crack is studied comprehensively. Firstly, the solution of a half-plane containing an arbitrary micro-crack and an edge macro-crack under mixed loads is presented in Sect. 2. The complete stress filed and SIFs are obtained. In Sect. 3, an FE model is established to compare with the theoretical solution and simulate the macro-crack propagation path. In Sect. 4, the effects of the micro-crack on stress field and macro-crack propagation rate and path are analyzed. In Sect. 5, some important conclusions are drawn.

2. Formulation

2.1. Problem Description

An elastic half-plane containing an edge macro-crack and an arbitrarily oriented micro-crack under uniform tension and shear loads is considered, as shown in Fig. 1. This problem can be divided into two subproblems. The first subproblem refers to an elastic half-plane without cracks under mixed loads, and the second one is an elastic half-plane containing continuously distributed dislocations in the crack regions without external loads.

2.2. Solution Scheme

For the first subproblem, the stress field can be given by

$$\tilde{\sigma}_{yy}(x,y) = \sigma^{\infty}, \ \tilde{\sigma}_{xy}(x,y) = \tau^{\infty}, \ \tilde{\sigma}_{xx}(x,y) = 0 \tag{1}$$

where σ^{∞} and τ^{∞} are the applied tension and shear loads, respectively, and $\tilde{\sigma}_{ij}$ denote the stress components contributed by the applied loads. The second subproblem will be presented in detail. For an edge dislocation located at $(\xi, 0)$ in an elastic half-plane, the stress components at (x, y) due to the dislocation can be given by

$$\bar{\sigma}_{ij}(x,y) = c\left[b_x G_{xij}(\xi,x,y) + b_y G_{yij}(\xi,x,y)\right], \ c = \frac{2\mu}{\pi(\kappa+1)}(ij = xx, \ xy \ or \ yy) \tag{2}$$

where μ and κ are the material constants; $\bar{\sigma}_{ij}$ denote the stress components contributed by the distributed dislocations; b_x and b_y are components of the Burgers vector; and the first subscript on $\boldsymbol{G}$ denotes the Burgers vector. The expressions of $G(\xi,x,y)$ can be obtained from [13]. For convenience, the macro-crack and the micro-crack are described as crack 1 and crack 2, respectively. By setting $y = 0$ for Eq. (2), the stresses along crack 1 induced by the dislocation located at crack 1 can be obtained as

$$\bar{\sigma}_{ij}^{11}(x) = c\left[b_x G_{xij}^{11}(\xi,x,0) + b_y G_{yij}^{11}(\xi,x,0)\right](ij = xx, \ xy \ or \ yy) \tag{3}$$

A local coordinate system $x' - o' - y'$ is established, as shown in Fig. 1. The local coordinate system is related to the global one by

$$\begin{aligned} x &= l + d\cos\theta + x'\cos\alpha - y'\sin\alpha \\ y &= d\sin\theta + x'\sin\alpha + y'\cos\alpha \end{aligned} \tag{4}$$

where l is the length of the macro-crack; θ is the micro-crack orientation; α is the micro-crack angle; and d is the distance between the macro-crack tip and the micro-crack center. The stress field in the local coordinate system can be obtained by

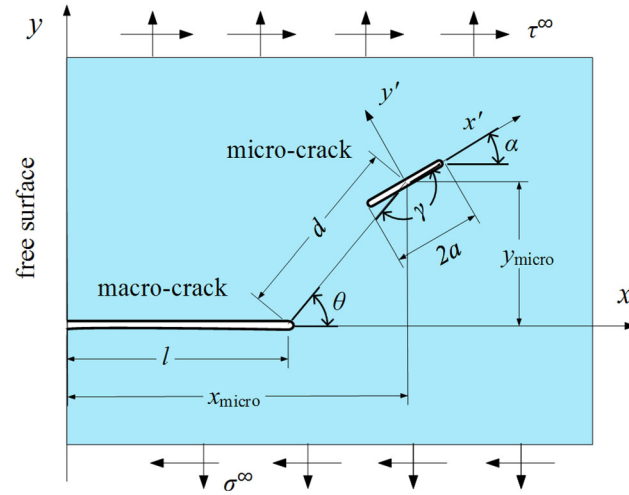$$\bar{\sigma}_{ij}(x',y') = c\left[b_x G_{xij}(\xi,x',y') + b_y G_{yij}(\xi,x',y')\right], \ ij = x'x', \ x'y' \ or \ y'y' \tag{5}$$

Fig. 1. A half-plane containing an edge macro-crack and an arbitrarily located micro-crack under mixed loads

where

$$G_{ix'x'}(\xi, x', y') = G_{ixx}(\xi, x, y)\cos^2\alpha + G_{iyy}(\xi, x, y)\sin^2\alpha + G_{ixy}(\xi, x, y)\sin 2\alpha$$
$$G_{iy'y'}(\xi, x', y') = G_{ixx}(\xi, x, y)\sin^2\alpha + G_{iyy}(\xi, x, y)\cos^2\alpha - G_{ixy}(\xi, x, y)\sin 2\alpha$$
$$G_{ix'y'}(\xi, x', y') = [G_{iyy}(\xi, x, y) - G_{ixx}(\xi, x, y)]\sin\alpha\cos\alpha + G_{ixy}(\xi, x, y)\cos 2\alpha$$
$$(i = x \text{ or } y) \tag{6}$$

Setting $y' = 0$ for Eq. (5), the stress components along crack 2 induced by the dislocation located at crack 1 can be obtained as

$$\bar{\sigma}_{ij}^{12}(x') = c\left[b_x G_{xij}^{12}(\xi, x', 0) + b_y G_{yij}^{12}(\xi, x', 0)\right] (ij = x'x',\ x'y' \text{ or } y'y') \tag{7}$$

In the same way, the stress components $\bar{\sigma}_{ij}^{21}(x)$ and $\bar{\sigma}_{ij}^{22}(x')$ can be obtained. After the stresses induced by an edge dislocation are obtained, the stresses induced by an array of edge dislocations along the crack line can be calculated by integration.

$$\bar{\sigma}_{ij}(x) = c\int_0^l \left[B_x^1(\xi)G_{xij}^{11}(\xi, x, 0) + B_y^1(\xi)G_{yij}^{11}(\xi, x, 0)\right]d\xi$$
$$+ c\int_{-a}^a \left[B_{x'}^2(\xi')G_{x'ij}^{21}(\xi', x, 0) + B_{y'}^2(\xi')G_{y'ij}^{21}(\xi', x, 0)\right]d\xi' \qquad (ij = xy \text{ or } yy)$$

$$\bar{\sigma}_{ij}(x') = c\int_0^l \left[B_x^1(\xi)G_{xij}^{12}(\xi, x', 0) + B_y^1(\xi)G_{yij}^{12}(\xi, x', 0)\right]d\xi$$
$$+ c\int_{-a}^a \left[B_{x'}^2(\xi')G_{x'ij}^{22}(\xi', x', 0) + B_{y'}^2(\xi')G_{y'ij}^{22}(\xi', x', 0)\right]d\xi' \qquad (ij = x'y' \text{ or } y'y') \tag{8}$$

where a is the half-length of the micro-crack; the superscript of $B(\xi)$ denotes the crack; and the subscript denotes the Burgers vector. For the problem shown in Fig. 1, it must be ensured that the crack faces are traction-free. So the following equations can be established.

$$\tilde{\sigma}_{ij}(x) + \bar{\sigma}_{ij}(x) = 0 \qquad (0 < x < l, \quad ij = yy \text{ or } xy)$$
$$\tilde{\sigma}_{ij}(x') + \bar{\sigma}_{ij}(x') = 0 \quad (-a < x' < a, \quad ij = y'y' \text{ or } x'y') \tag{9}$$

Substituting Eq. (8) into Eq. (9), the integral equations are established. The numerical solution of Eq. (9) can be obtained by the Gauss–Chebyshev quadrature method [13, 40, 41]. Letting $\xi = 0.5ls + 0.5l$, $x = 0.5lt + 0.5l$, $\xi' = as'$ and $x' = at'$ (s and s' are discrete integration points; t and t' are collocation points), the integral intervals $[0, l]$ and $[-a, a]$ can be normalized to interval $[-1, 1]$. In the present problem, the half-plane contains an edge macro-crack and a centric micro-crack. The

centric micro-crack is singular at both ends, so the form of the dislocation density function can be set as

$$B(s') = \phi(s')/\sqrt{(1-s')(1+s')} \tag{10}$$

The edge macro-crack is singular at the crack tip but bounded at the other end, so the form of the dislocation density function can be set as

$$B(s) = \phi(s)\sqrt{1+s}/\sqrt{1-s} \tag{11}$$

$\phi(s)$ and $\phi(s')$ are unknown functions. Equation (9) can be replaced approximately by a series of algebraic equations based on the numerical method. It can be written as

$$-\tilde{\sigma}_{ij}(t_K)\frac{\kappa+1}{2\mu} = 0.5l\sum_{I=1}^{N}\frac{(1+s_I)}{2N+1}\left[\phi_x^1(s_I)G_{xij}^{11}(s_I,t_K) + \phi_y^1(s_I)G_{yij}^{11}(s_I,t_K)\right]$$

$$+ a\sum_{I=1}^{N}\frac{1}{N}\left[\phi_{x'}^2(s_I')G_{x'ij}^{21}(s_I',t_K) + \phi_{y'}^2(s_I')G_{y'ij}^{21}(s_I',t_K)\right](ij = xy \text{ or } yy)$$

$$-\tilde{\sigma}_{ij}(t_K')\frac{\kappa+1}{2\mu} = 0.5l\sum_{I=1}^{N}\frac{(1+s_I)}{2N+1}\left[\phi_x^1(s_I)G_{xij}^{12}(s_I,t_K') + \phi_y^1(s_I)G_{yij}^{12}(s_I,t_K')\right]$$

$$+ a\sum_{I=1}^{N}\frac{1}{N}\left[\phi_{x'}^2(s_I')G_{x'ij}^{22}(s_I',t_K') + \phi_{y'}^2(s_I')G_{y'ij}^{22}(s_I',t_K')\right](ij = x'y' \text{ or } y'y') \tag{12}$$

where

$$s_I' = \cos\left[\pi\frac{2I-1}{2N}\right](I = 1...N;\ t_K' = \cos\left[\frac{\pi K}{N}\right],\quad K = 1...N-1)$$

$$s_I = \cos\left[\pi\frac{2I-1}{2N+1}\right](I = 1...N;\ t_K = \cos\left[\frac{2\pi K}{2N+1}\right],\quad K = 1...N) \tag{13}$$

where N is the number of discrete integration points. The selection of N has a significant effect on the computational accuracy, which will be discussed later. There are $4N$ unknown functions of $\phi(s_I)$ and $\phi(s_I')$ in Eq. (12), but only $4N-2$ algebraic equations. Two extra equations must be established. On the micro-crack, there is no net dislocation. So

$$\sum_{I=1}^{N}\phi_{x'}^2(s_I') = \sum_{I=1}^{N}\phi_{y'}^2(s_I') = 0 \tag{14}$$

where the superscript of ϕ_i^2 denotes the crack. Combining Eqs. (12) and (14), the unknown functions $\phi(s_I)$ and $\phi(s_I')$ can be obtained. So the SIFs at the macro-crack tip can be given by

$$K_{\text{I,II}} = c\sqrt{\pi l}\sqrt{2}\phi_{y,x}^1 \tag{15}$$

where the superscript of ϕ_i^1 denotes the crack, and

$$\phi_i^1 = \frac{2}{2N+1}\sum_{I=1}^{N}\phi_i^1(s_I)\cot\left[\pi\frac{2I-1}{4N}\right]\sin\left[N\pi\frac{2I-1}{2N+1}\right]\quad (i = x \text{ or } y) \tag{16}$$

The stress field in the global coordinate system can be obtained by superposition of three parts, that is

$$\sigma_{ij}(x,y) = \tilde{\sigma}_{ij}(x,y) + \bar{\sigma}_{ij}^1(x,y) + \bar{\sigma}_{ij}^2(x,y)\quad (ij = xx,\ xy \text{ or } yy) \tag{17}$$

where $\tilde{\sigma}_{ij}$ is the stress components induced by the applied loads; $\bar{\sigma}_{ij}^1$ is the stress components induced by the dislocations distributed on the macro-crack; and $\bar{\sigma}_{ij}^2$ is the stress components induced by the

dislocations distributed on the micro-crack. Thus, the stress field can be given by an integral formula, i.e.,

$$\sigma_{ij}(x,y) = \tilde{\sigma}_{ij}(x,y) + \frac{2\mu}{\pi(\kappa+1)} \int_0^l \left[B_x^1(\xi)G_{xij}^{11}(\xi,x,y) + B_y^1(\xi)G_{yij}^{11}(\xi,x,y) \right] \mathrm{d}\xi$$
$$+ \frac{2\mu}{\pi(\kappa+1)} \int_{-a}^{a} \left[B_{x'}^2(\xi')G_{x'ij}^{21}(\xi',x,y) + B_{y'}^2(\xi')G_{y'ij}^{21}(\xi',x,y) \right] \mathrm{d}\xi' \quad (ij = xy \text{ or } yy) \,(18)$$

Based on the Gauss–Chebyshev quadrature method, the integral terms in Eq. (18) can be discretized.

$$\sigma_{ij}(x,y) = \tilde{\sigma}_{ij}(x,y) + \frac{l\mu}{\kappa+1} \sum_{I=1}^N \frac{(1+s_I)}{2N+1} \begin{bmatrix} \phi_x^1(s_I)G_{xij}(0.5ls_I + 0.5l, x, y) \\ \phi_y^1(s_I)G_{yij}(0.5ls_I + 0.5l, x, y) \end{bmatrix}$$
$$+ \frac{2a\mu}{\kappa+1} \sum_{I=1}^N \frac{1}{N} \begin{bmatrix} \phi_{x'}^2(s_I')G_{x'ij}(as_I', x, y) + \\ \phi_{y'}^2(s_I')G_{y'ij}(as_I', x, y) \end{bmatrix} \quad (ij = xx,\ xy \text{ or } yy) \qquad (19)$$

where the superscript of ϕ denotes the crack, and $\phi^1(s_I)$ and $\phi^2(s_I')$ have been obtained by solving Eqs. (12) and (14).

Considering the case of plane stress, the von Mises stress can be given by

$$\sigma_{\mathrm{von}} = \sqrt{0.5\left[(\sigma_1 - \sigma_2)^2 + (\sigma_2)^2 + (\sigma_1)^2\right]}$$
$$\sigma_{1,2} = 0.5(\sigma_{xx} + \sigma_{yy}) \pm 0.5\sqrt{(\sigma_{xx} - \sigma_{yy})^2 + 4\sigma_{xy}^2} \qquad (20)$$

where σ_1 and σ_2 are the first and second principal stresses, respectively.

2.3. Crack Propagation Direction and Rate

Erdogan and Sih [24] proposed the MCTSC. It was described that the crack propagates along the direction where the circumferential tensile stress is maximum. According to the criterion, the crack propagation direction can be given by

$$\beta = -\arccos\left(\frac{3K_{\mathrm{II}}^2 + K_{\mathrm{I}}\sqrt{K_{\mathrm{I}}^2 + 8K_{\mathrm{II}}^2}}{K_{\mathrm{I}}^2 + 9K_{\mathrm{II}}^2}\right) \qquad (21)$$

There is a positive correlation between crack propagation rate and the SIF at crack tip. For a mixed-mode crack, the ESIF is applied to represent the combination action of K_{I} and K_{II}. The expression of ESIF can be given by [42–45]:

$$K_{\mathrm{eff}} = \sqrt{K_{\mathrm{I}}^2 + 2K_{\mathrm{II}}^2} \qquad (22)$$

The ESIF will be applied to qualitatively analyze the crack propagation rate in this paper.

3. FE Simulation

As shown in Fig. 2, a two-dimensional FE model is established. The material parameters are $E = 210$ GPa and $\nu = 0.3$. The element type is PLANE183. It is singular at the crack tips, so the classical singular element is applied at the crack tips. There are 20 elements around the crack tips. The initial length of the macro-crack is 1 mm. The elements near the crack are about 0.01 mm. The length of the model is 60 mm, which is sufficiently large in comparison with the macro-crack length. So the model can be considered as a half-infinite plane. The model is subjected to uniaxial uniform tensile load. The FE calculation is elastic.

The purposes of FE simulation are to verify the theoretical solution and to simulate the macro-crack propagation path.

Two cases will be considered to verify the theoretical solution.

(a) Considering the case that a half-plane contains a micro-crack of different orientation near the macro-crack tip under uniaxial tensile load, SIFs are used to measure the validity of the theoretical solution.
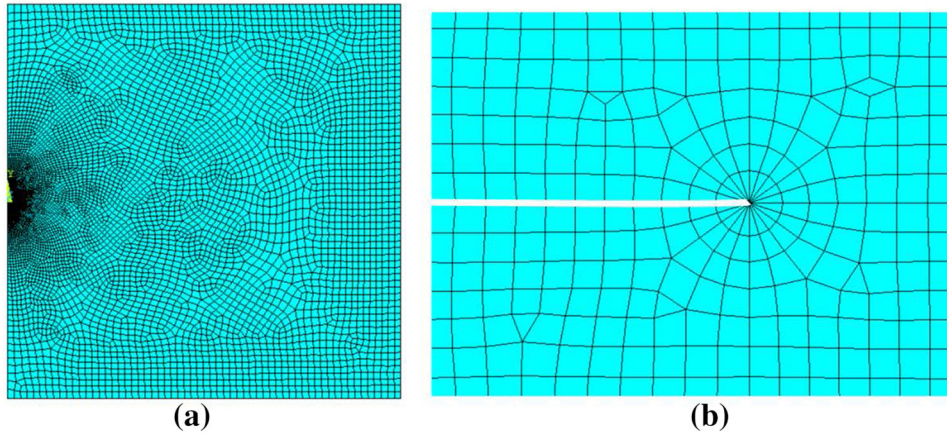
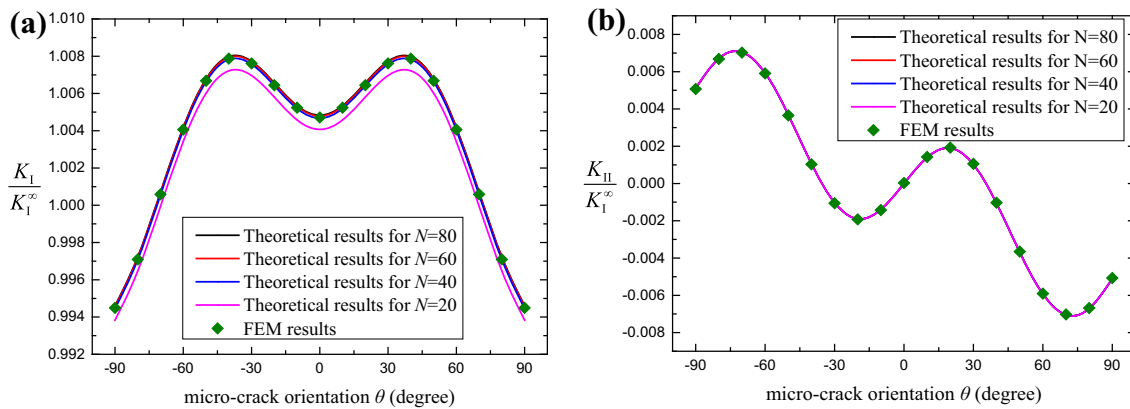Fig. 2. FE model: **a** global model; **b** FE meshes at the crack tip

Fig. 3. Comparison of SIFs between theoretical and simulated results under uniaxial tensile load: **a** mode I SIF; **b** mode II SIF. The parameters are $a/l = 1/40$, $\alpha = 0°$ and $d/l = 0.2$

(b) Considering the case of a half-plane containing only a macro-crack under uniaxial tensile load, the von Mises stress field is used to measure the validity of the theoretical solution.

The other purpose of FE simulation is to analyze the macro-crack propagation path. The calculation procedures are as follows:

1. The FE model is established. The SIFs are calculated by the interaction integral method.
2. The macro-crack propagation direction β is calculated by Eq. (21).
3. The macro-crack propagates 0.05 mm along the direction β, and the element re-meshing is carried out.
4. Go to Step 1.

When the effect of the micro-crack is very small or the micro-crack and the macro-crack join, the calculation stops.

4. Results and Discussion

4.1. Verification and Comparison of Results

4.1.1. Comparison of SIFs

The variation of normalized SIFs versus the micro-crack orientation is depicted. The comparison between theoretical and simulated results is shown in Fig. 3. The results show that the theoretical results are very close to the FEM results, which verifies the theoretical solution.
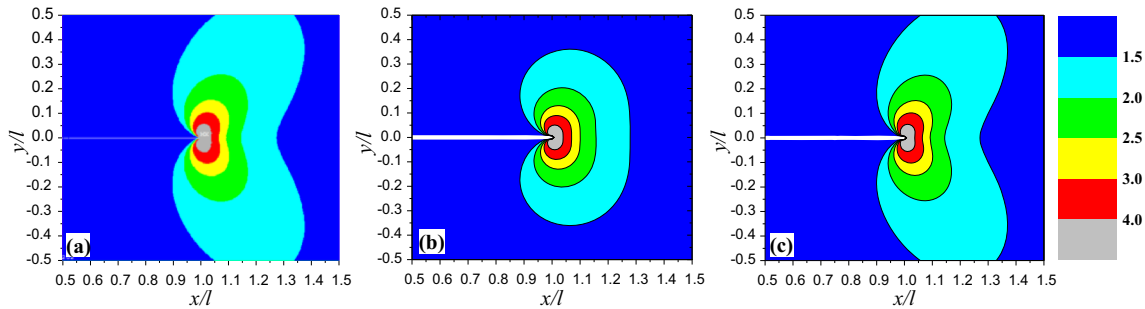
Fig. 4. Comparison of normalized von Mises stress field $\sigma_{\text{von}}/\sigma^\infty$ between theoretical and simulated results under uniaxial tensile load: **a** FEM; **b** conventional fracture mechanics; **c** theoretical solution in the paper

The number of discrete integration points N has a relatively large effect on mode I SIF, but has little effect on mode II SIF in this case. The difference between the theoretical and simulated results is very small when the number of discrete integration points is larger than 40 ($N > 40$). In this paper, N is taken as 80, so the theoretical results are sufficiently accurate.

4.1.2. Comparison of Stress Field

The contour of normalized von Mises stress is depicted. The comparison between the results of FEM, conventional fracture mechanics and theoretical analysis is shown in Fig. 4. It shows that the theoretical stress field is highly consistent with the FEM results. The results in Figs. 3 and 4 illustrate the validity of theoretical and simulated methods in this paper.

In the conventional fracture mechanics, the higher-order terms of crack tip stress field are neglected, and the opening-mode crack tip stress field can be given by

$$\sigma_{xx} = \frac{K_{\text{I}}}{\sqrt{2\pi\rho}} \cos\frac{\varphi}{2} \left(1 - \sin\frac{\varphi}{2}\sin\frac{3\varphi}{2}\right)$$

$$\sigma_{yy} = \frac{K_{\text{I}}}{\sqrt{2\pi\rho}} \cos\frac{\varphi}{2} \left(1 + \sin\frac{\varphi}{2}\sin\frac{3\varphi}{2}\right)$$

$$\sigma_{xy} = \frac{K_{\text{I}}}{\sqrt{2\pi\rho}} \cos\frac{\varphi}{2} \sin\frac{\varphi}{2} \cos\frac{3\varphi}{2} \tag{23}$$

where $\rho = \sqrt{(x-l)^2 + y^2}$, $\varphi = \arctan\left[y/(x-l)\right]$ $(x \geq l)$, $\varphi = \arctan\left[y/(x-l)\right] + \pi$ $(x < l)$. By substituting Eq. (23) into Eq. (20), the von Mises stress field near the crack tip can be obtained.

Recent studies [46–51] showed that the T-stress and higher-order terms had significant effects on crack propagation. The stress field in this paper is the complete stress field, which is more accurate than the conventional fracture mechanics and the stress field considering T-stress. For small-scale yielding, the elastic stress field can be applied to predict the shape of plastic zone based on some yield criteria. The complete stress field is more accurate for the prediction of plastic zone.

4.2. Theoretical Results

4.2.1. Influence of Micro-crack Length on ESIF

The variation of normalized ESIF versus micro-crack length for different micro-crack orientations is shown in Fig. 5. The results show that the effect of the micro-crack on the macro-crack propagation rate increases with the increase in micro-crack length. The micro-crack has the shielding effect on the macro-crack propagation at $\theta = 75°$, but the amplifying effect at $\theta = 15°$, $30°$ and $45°$. The micro-crack has little effect on the macro-crack at $\theta = 60°$.

4.2.2. Shielding and Amplifying Effects of the Micro-crack

The variation of normalized ESIF versus the normalized micro-crack location $(x_{\text{micro}}/l, y_{\text{micro}}/l)$ for different micro-crack angles under uniaxial tensile load is shown in Fig. 6. The results show that the shielding effect regions are like two 'petals.' As the micro-crack angle changes, the shielding effect regions rotate. In order to summarize the law handily, a parameter γ is defined as the intersection
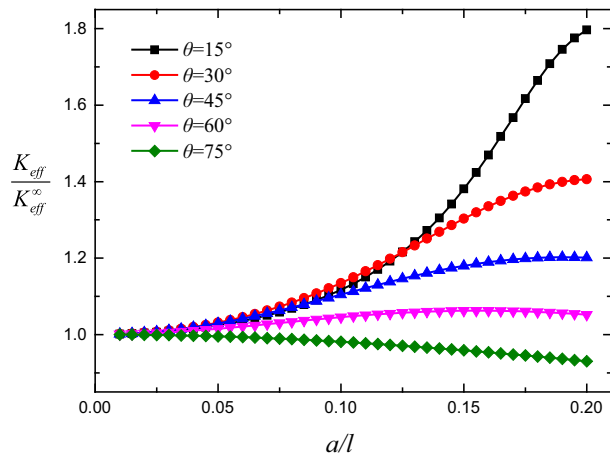
Fig. 5. ESIF versus micro-crack length under uniaxial tensile load. The parameters are $\alpha = 0°$ and $d/l = 0.2$

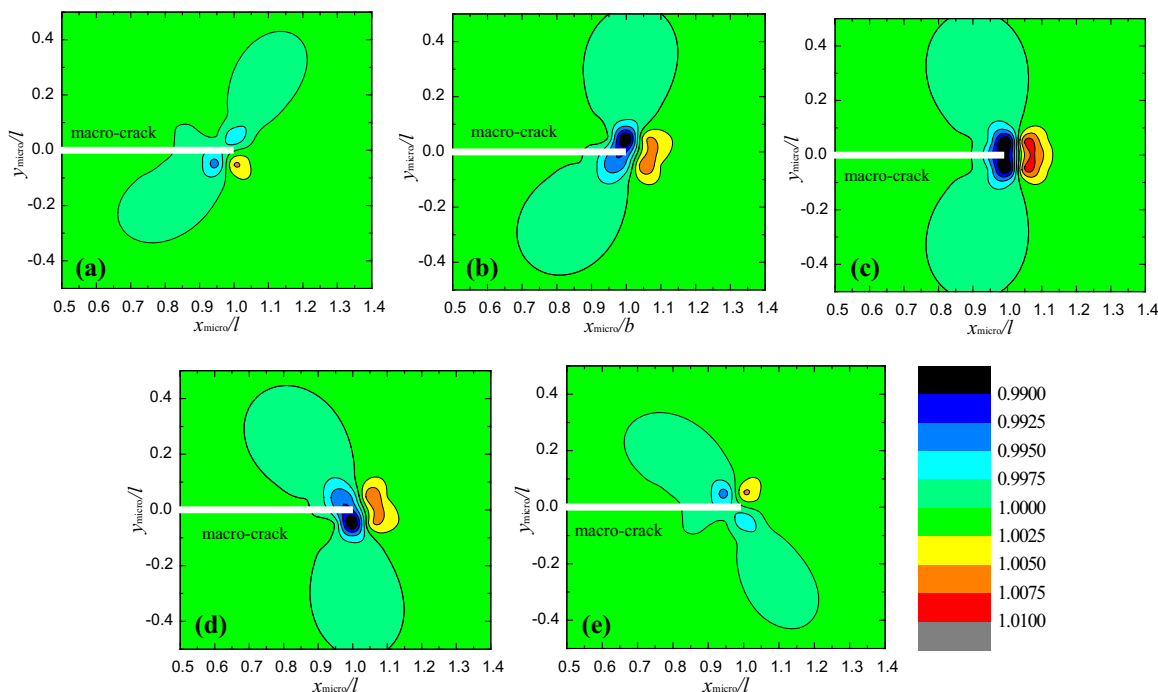Fig. 6. Contour of normalized ESIF $K_{\text{eff}}/K_{\text{eff}}^\infty$ under uniaxial tensile load: **a** $\alpha = -60°$; **b** $\alpha = -30°$; **c** $\alpha = 0°$; **d** $\alpha = 30°$; **e** $\alpha = 60°$. The parameter a/l is taken as 0.01. The macro-crack is located in $[0, l]$, and the micro-crack center is located at $(x_{\text{micro}}, y_{\text{micro}})$

angle between the micro-crack face and the line composed by the micro-crack center and macro-crack tip, as shown in Fig. 1. In fact, the results in Fig. 6 can be summarized that the micro-crack has the shielding effect at about $\gamma = 90°$. Firstly, considering $\alpha = 0°$ (Fig. 6c), the shielding effect regions are symmetric. The micro-crack has the shielding effect when it is located at the top or bottom of the macro-crack tip, and γ is about 90° in this case. Considering $\alpha = 30°$ (Fig. 6d), the shielding effect regions rotate about 30° counterclockwise in comparison with Fig. 6c. In this case, the angle γ is also about 90°. Considering Fig. 6a–e, the same law applies, i.e., the micro-crack has the shielding effect at about $\gamma = 90°$ under uniaxial tensile load. This is because the micro-crack face has the shielding effect.
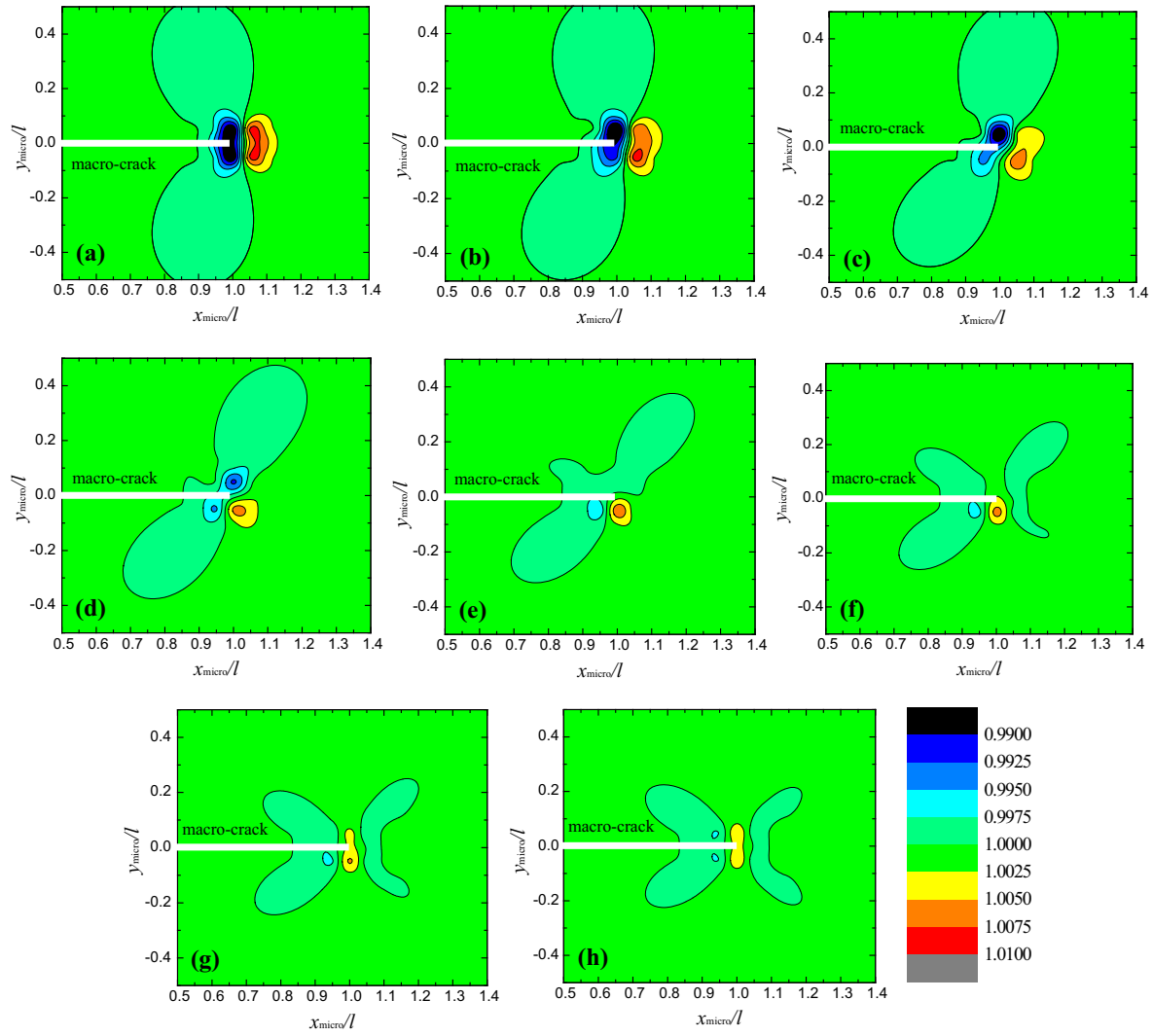
Fig. 7. Contour of normalized ESIF $K_{\mathrm{eff}}/K_{\mathrm{eff}}^{\infty}$ under mixed loads: **a** $\tau^{\infty} = 0$; **b** $\tau^{\infty}/\sigma^{\infty} = 0.2$; **c** $\tau^{\infty}/\sigma^{\infty} = 0.5$; **d** $\tau^{\infty}/\sigma^{\infty} = 1$; **e** $\tau^{\infty}/\sigma^{\infty} = 2$; **f** $\tau^{\infty}/\sigma^{\infty} = 5$; **g** $\tau^{\infty}/\sigma^{\infty} = 10$; **h** $\sigma^{\infty} = 0$. The other parameters are $\alpha = 0°$ and $a/l = 1/100$. The macro-crack is located in $[0, l]$, and the micro-crack center is located at $(x_{\mathrm{micro}}, y_{\mathrm{micro}})$

The effect of the micro-crack on the ESIF becomes weaker as the inclination of micro-crack (the absolute value of α) increases. This means the parallel micro-crack has a greater contribution to the ESIF than the inclined micro-crack.

The variation of normalized ESIF versus the normalized micro-crack location $(x_{\mathrm{micro}}/l, y_{\mathrm{micro}}/l)$ for different $\tau^{\infty}/\sigma^{\infty}$ under mixed loads is shown in Fig. 7. The results show that the shielding effect regions rotate clockwise with the increase in ratio $\tau^{\infty}/\sigma^{\infty}$. The shielding effect regions are like two 'petals' when $\tau^{\infty}/\sigma^{\infty} \leq 2$, and split into two parts from the macro-crack tip when $\tau^{\infty}/\sigma^{\infty} \geq 5$. The effect of the micro-crack on the ESIF increases with the decrease in distance d. The closer is the micro-crack location, the greater is the effect on the macro-crack. The effect of the micro-crack on the ESIF becomes weaker as the ratio $\tau^{\infty}/\sigma^{\infty}$ increases. This means the tensile load has a greater contribution to the interaction between micro-crack and macro-crack than the shear load.

4.2.3. The von Mises Stress Field Affected by a Micro-crack

The variation of normalized von Mises stress field near the macro-crack tip versus the micro-crack location under uniaxial tensile load is depicted in Fig. 8. The results in Fig. 8a, d show that the
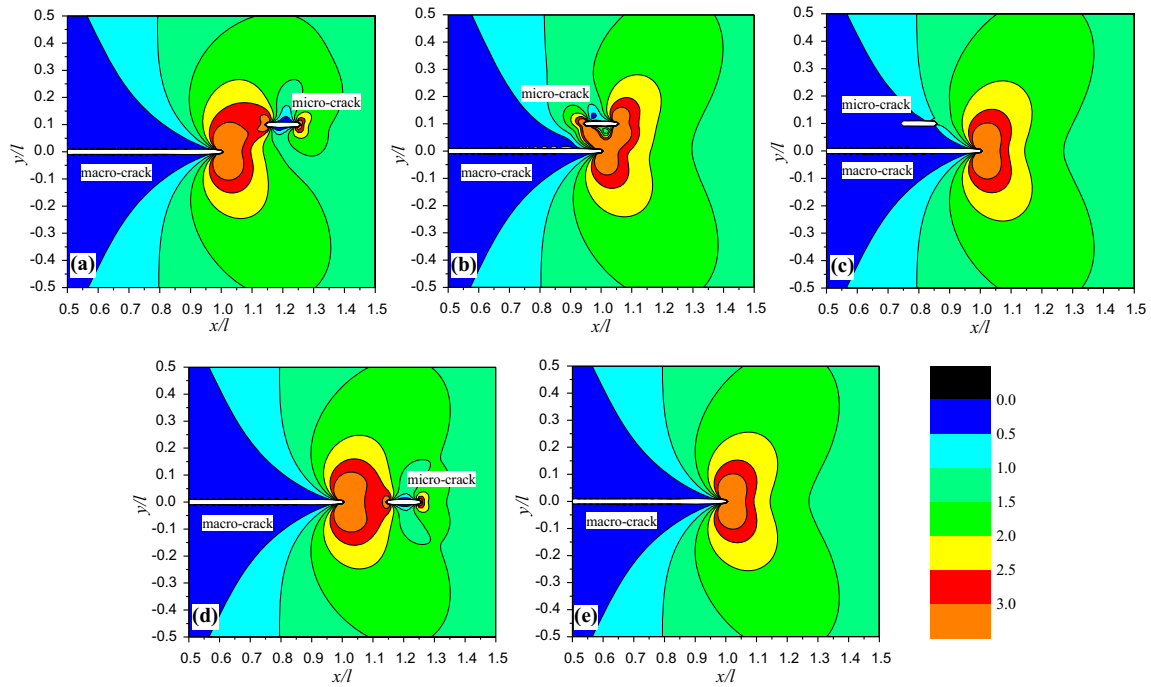
Fig. 8. Influence of the micro-crack on the normalized von Mises stress field $\sigma_{\mathrm{von}}/\sigma^{\infty}$ under uniaxial tensile load: **a** $(x_{\mathrm{micro}}, y_{\mathrm{micro}}) = (1.2l, 0.1l)$; **b** $(x_{\mathrm{micro}}, y_{\mathrm{micro}}) = (l, 0.1l)$; **c** $(x_{\mathrm{micro}}, y_{\mathrm{micro}}) = (0.8l, 0.1l)$; **d** $(x_{\mathrm{micro}}, y_{\mathrm{micro}}) = (1.2l, 0)$; **e** without micro-crack. The macro-crack location is from 0 to l

red regions in the stress field enlarge when the micro-crack is located in front of the macro-crack tip; namely, the micro-crack aggravates the stress concentration in this case. The results in Fig. 6c show the amplifying effect of micro-crack on the ESIF when it is located in front of the macro-crack tip, which is consistent with Fig. 8. The results of Fig. 8b show that the red regions split into two parts when the micro-crack is located in the red regions. In fact, in this case, the stress field near the macro-crack tip is released and the stress concentration is partially relaxed. The results in Fig. 6c also show the shielding effect of micro-crack on the ESIF when it is located at the top of the macro-crack tip. The results in Fig. 8c show that the micro-crack has little effect on the stress field when it is located behind the macro-crack tip.

The variation of normalized von Mises stress field near the macro-crack tip versus the micro-crack location under mixed loads is depicted in Fig. 9, which shows similar results as in Fig. 8. Figure 9d, g shows that the micro-crack aggravates the stress concentration when it is located in front of the macro-crack tip. The results in Fig. 9a, b, e show that the red regions split into two parts when the micro-crack is located in the red regions. In this case, the stress field near the macro-crack tip is released and the stress concentration is partially relaxed. The results in Fig. 9c, f show that the micro-crack has little effect on the stress field near the macro-crack tip when it is located behind the macro-crack tip. The conclusions from the results in Fig. 9 are consistent with those from Fig. 7c. The ESIF is a parameter to represent the stress concentration, so similar conclusions can be drawn from the analyses of ESIF and stress field.

4.3. Simulation Results

4.3.1. The Macro-crack Propagation Path Affected by a Micro-crack

The variation of macro-crack propagation path with micro-crack under uniaxial tensile load is shown in Fig. 10. The macro-crack propagates along the original direction without the micro-crack. The results show an increasing effect of the micro-crack on the macro-crack propagation with the decrease in vertical distance. In all cases of Fig. 10, the micro-crack has an attraction effect on the macro-crack propagation path. This is similar to the attraction effect of soft inclusion on crack propagation
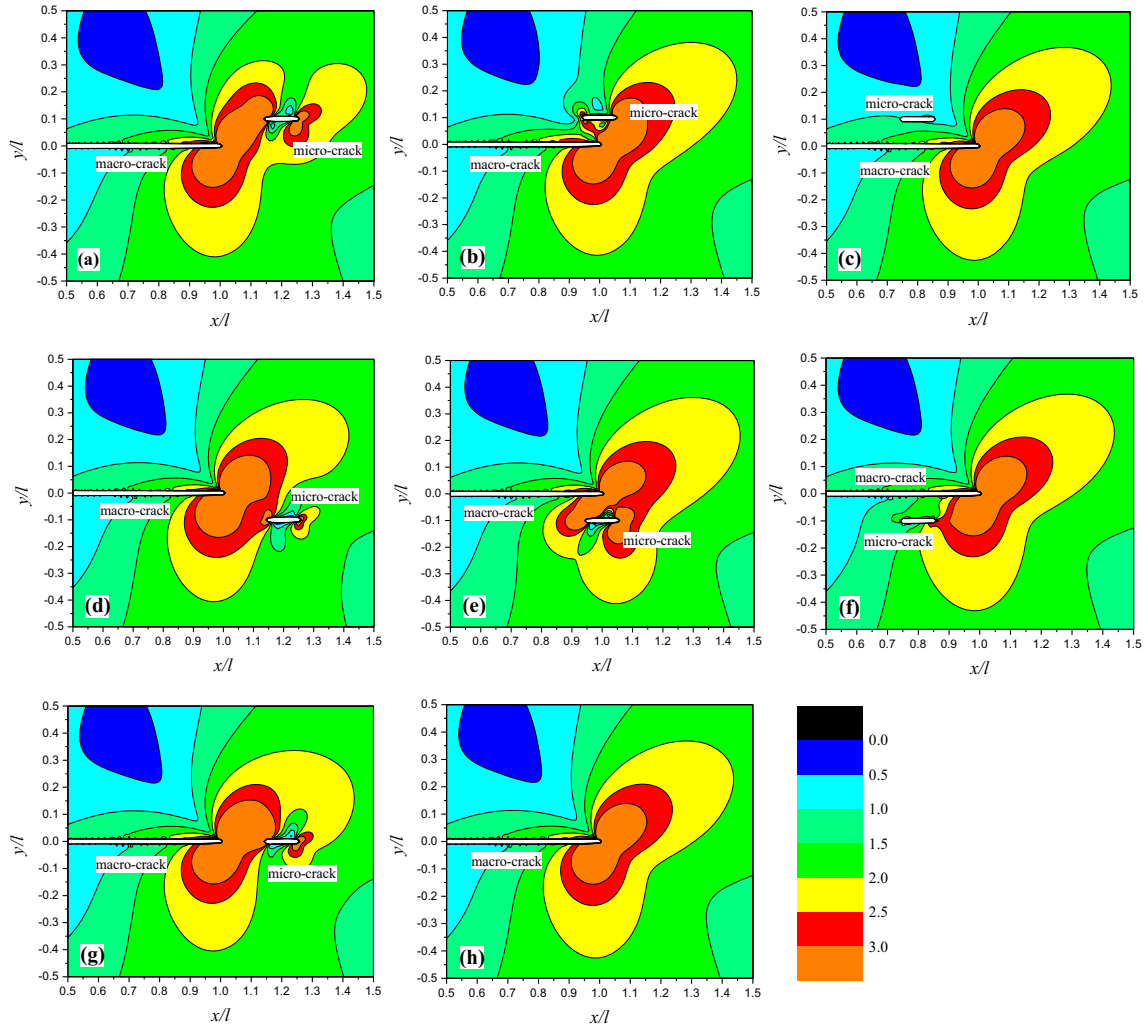
Fig. 9. Influence of the micro-crack on the normalized von Mises stress field $\sigma_{\mathrm{von}}/\sigma^{\infty}$ under mixed loads ($\tau^{\infty}/\sigma^{\infty} = 0.5$): **a** ($x_{\mathrm{micro}}$, y_{micro}) = ($1.2l$, $0.1l$); **b** (x_{micro}, y_{micro}) = ($l, 0.1l$); **c** (x_{micro}, y_{micro}) = ($0.8l, 0.1l$); **d** (x_{micro}, y_{micro}) = ($1.2l, -0.1l$); **e** (x_{micro}, y_{micro}) = (l, -$0.1l$); **f** (x_{micro}, y_{micro}) = ($0.8l, -0.1l$); **g** (x_{micro}, y_{micro}) = ($1.2l$, 0); **h** without micro-crack. The macro-crack location is from 0 to l

[29, 52, 53]. For the cases of $\alpha = 0°$ and $\alpha = -45°$, the macro-crack and micro-crack join when the vertical distance decreases to a certain extent. When $\alpha = 45°$, however, the micro-crack deflects the macro-crack propagation greatly. In this case, the micro-crack tip and macro-crack tip are very close, so the effect on macro-crack is great. When the macro-crack propagates through the micro-crack, the macro-crack propagation direction is close to the horizontal direction.

4.3.2. The Macro-crack Propagation Rate Affected by a Micro-crack

The variation of ESIF with micro-crack under uniaxial tensile load is depicted in Fig. 11. The results show that, during the process of macro-crack propagation, the macro-crack propagation rate increases first, then decreases, and then increases again. Initially, the micro-crack is located in front of the macro-crack. Based on the analysis of Sect. 4.2, the micro-crack has an amplifying effect on the macro-crack propagation. After that, with the propagation of macro-crack, the macro-crack tip is located at the bottom of the micro-crack face and has a shielding effect on the macro-crack propagation. Finally, the macro-crack propagation rate is close to the curve of 'no micro-crack' because the micro-crack has little effect when it is located behind the macro-crack tip, so the micro-crack has little effect on the macro-crack propagation direction and rate when the macro-crack propagates through it.
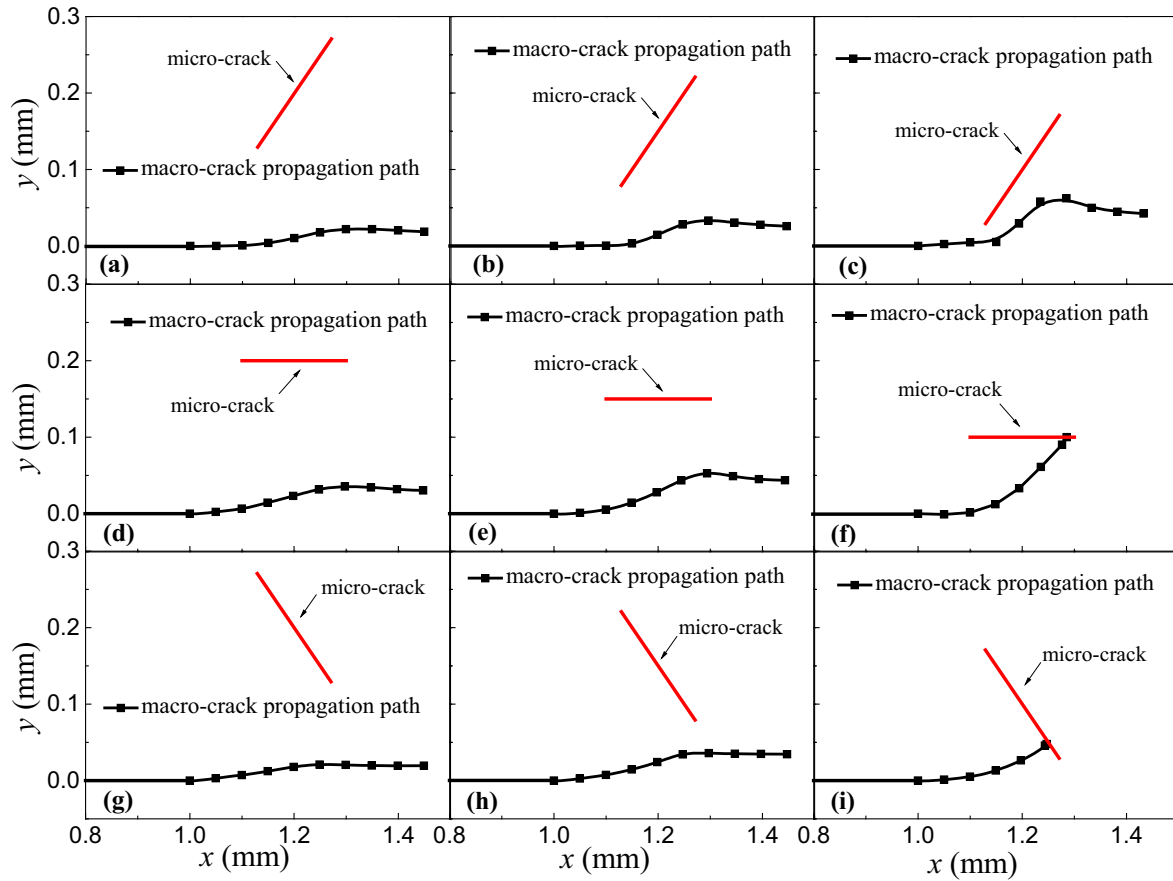
Fig. 10. Influence of a micro-crack on the macro-crack propagation path under uniaxial tensile load: **a** $y_{\mathrm{micro}} = 0.2$ mm and $\alpha = 45°$; **b** $y_{\mathrm{micro}} = 0.15$ mm and $\alpha = 45°$; **c** $y_{\mathrm{micro}} = 0.1$ mm and $\alpha = 45°$; **d** $y_{\mathrm{micro}} = 0.2$ mm and $\alpha = 0°$; **e** $y_{\mathrm{micro}} = 0.15$ mm and $\alpha = 0°$; **f** $y_{\mathrm{micro}} = 0.1$ mm and $\alpha = 0°$; **g** $y_{\mathrm{micro}} = 0.2$ mm and $\alpha = -45°$; **h** $y_{\mathrm{micro}} = 0.15$ mm and $\alpha = -45°$; **i** $y_{\mathrm{micro}} = 0.1$ mm and $\alpha = -45°$. The micro-crack length is taken as 0.2 mm. The initial length of the macro-crack is 1 mm. The parameter x_{micro} is 1.2 mm

Fig. 11. Variation of ESIF in the process of macro-crack propagation: **a** $\alpha = 45°$; **b** $\alpha = 0°$; (c) $\alpha = -45°$. The micro-crack length is taken as 0.2 mm. The initial length of the macro-crack is 1 mm. The parameter x_{micro} is 1.2 mm
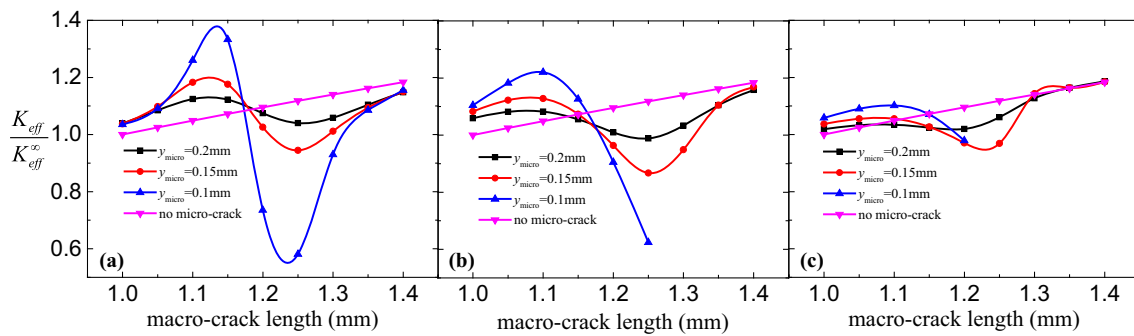
5. Conclusions

In this study, the complete stress field and SIFs are obtained via theoretical derivation. The stress field is more accurate than the conventional fracture mechanics. The macro-crack propagation path is simulated. The effect of a micro-crack on the edge macro-crack propagation rate and path under mixed loads is analyzed in detail based on the theoretical and FEM results. Some important conclusions are drawn as follows.

(1) The shielding effect region is like two 'petals' under uniaxial tensile load and rotates with the change in micro-crack angle.
(2) The shielding effect region rotates clockwise with the increase in ratio $\tau^\infty/\sigma^\infty$. It is like two 'petals' when $\tau^\infty/\sigma^\infty \leq 2$ and splits into two parts from the macro-crack tip when $\tau^\infty/\sigma^\infty \geq 5$.
(3) The micro-crack aggravates the stress concentration when it is located in front of the macro-crack tip. The stress concentration is partially relaxed when the micro-crack is located at the top or bottom of the macro-crack tip. The micro-crack has little effect on the stress field when it is located behind the macro-crack tip.
(4) The effect of the micro-crack on the macro-crack increases with the increase in micro-crack length. With the decrease in distance d, the micro-crack inclination decreases and the ratio $\tau^\infty/\sigma^\infty$ decreases.
(5) The micro-crack has the attraction effect on the macro-crack propagation. The micro-crack has little effect on the macro-crack propagation direction and rate when the macro-crack propagates through it.

The investigation of the effect of a micro-crack on the macro-crack propagation is important for predicting the fracture behaviors of structures containing micro-cracks. The macro-crack propagation rate can be lowered down by prefabricating micro-cracks in the shielding regions, so the analysis of shielding and amplifying effects can be useful for material design.

References

[1] Kachanov M. A simple technique of stress analysis in elastic solids with many cracks. Int J Fract. 1985;28:R11–9.
[2] Kachanov M. Elastic solids with many cracks: a simple method of analysis. Int J Solids Struct. 1987;23:23–43.
[3] Chudnovsky A, Dolgopolsky A, Kachanov M. Elastic interaction of a crack with a microcrack array: II. Elastic solution for two crack configurations (piecewise constant and linear approximations). Int J Solids Struct. 1987;23:11–21.
[4] Gong SX, Horii H. General solution to the problem of microcracks near the tip of a main crack. J Mech Phys Solids. 1989;37:27–46.
[5] Gong SX, Meguid SA. Microdefect interacting with a main crack: a general treatment. Int J Mech Sci. 1992;34:933–45.
[6] Gong SX. On the main crack-microcrack interaction under mode III loading. Eng Fract Mech. 1995;51:753–62.
[7] Tamuzs V, Petrova V. Modified model of macro-microcrack interaction. Theor Appl Fract Mech. 1999;32:111–7.
[8] Soh AK, Yang CH. Numerical modeling of interactions between a macro-crack and a cluster of micro-defects. Eng Fract Mech. 2004;71:193–217.
[9] Alam MM, Barsoum Z, Jonsén P, Kaplan AFH, Häggblad HÅ. Influence of defects on fatigue crack propagation in laser hybrid welded eccentric fillet joint. Eng Fract Mech. 2011;78:2246–58.
[10] Budyn É, Zi G, Moës N, Belytschko T. A method for multiple crack growth in brittle materials without remeshing. Int J Numer Methods Eng. 2004;61:1741–70.
[11] Bouiadjra BB, Benguediab M, Elmeguenni M, Belhouari M, Serier B, Aziz MNA. Analysis of the effect of micro-crack on the plastic strain ahead of main crack in aluminium alloy 2024 T3. Comput Mater Sci. 2008;42:100–6.
[12] Li X, Li X, Yang H, Jiang X. Effect of micro-cracks on plastic zone ahead of the macro-crack tip. J Mater Sci. 2017;52:13490–503.

[13] Hills D, Kelly P, Dai D, Korsunsky A. Solution of crack problems: the distributed dislocation technique, 1996. Dordrecht: Kluwer Academic Publishers; 1996.

[14] Jin X, Keer LM. Solution of multiple edge cracks in an elastic half plane. Int J Fract. 2006;137:121–37.

[15] Jin X. Analysis of some two dimensional problems containing cracks and holes. Northwestern University, 2006.

[16] Zhang J, Qu Z, Huang Q, Xie L, Xiong C. Solution of multiple cracks in a finite plate of an elastic isotropic material with the distributed dislocation method. Acta Mech Solida Sin. 2014;27:276–83.

[17] Li X, Jiang X, Li X, Yang H, Zhang Y. Solution of an inclined crack in a finite plane and a new criterion to predict fatigue crack propagation. Int J Mech Sci. 2016;119:217–23.

[18] Han J-J, Dhanasekar M. Modelling cracks in arbitrarily shaped finite bodies by distribution of dislocation. Int J Solids Struct. 2004;41:399–411.

[19] Erdogan F, Gupta G, Ratwani M. Interaction between a circular inclusion and an arbitrarily oriented crack. J Appl Mech. 1974;41:1007–13.

[20] Xiao Z, Bai J, Maeda R. Electro-elastic stress analysis on piezoelectric inhomogeneity-crack interaction. Int J Solids Struct. 2001;38:1369–94.

[21] Mousavi SM, Paavola J. Analysis of a cracked concrete containing an inclusion with inhomogeneously imperfect interface. Mech Res Commun. 2014;63:1–5.

[22] Tao Y, Fang Q, Zeng X, Liu Y. Influence of dislocation on interaction between a crack and a circular inhomogeneity. Int J Mech Sci. 2014;80:47–53.

[23] Zhang J, Qu Z, Huang Q, Xie L, Xiong C. Interaction between cracks and a circular inclusion in a finite plate with the distributed dislocation method. Arch Appl Mech. 2013;83:861–73.

[24] Erdogan F, Sih G. On the crack extension in plates under plane loading and transverse shear. J Fluids Eng. 1963;85:519–25.

[25] Palaniswamy K, Knauss W. Propagation of a crack under general, in-plane tension. Int J Fract. 1972;8:114–7.

[26] Sih GC. Strain-energy-density factor applied to mixed mode crack problems. Int J Fract. 1974;10:305–21.

[27] Li C. Vector CTD criterion applied to mixed mode fatigue crack growth. Fatigue Fract Eng Mater Struct. 1989;12:59–65.

[28] Khan SMA, Khraisheh MK. A new criterion for mixed mode fracture initiation based on the crack tip plastic core region. Int J Plast. 2004;20:55–84.

[29] Bouchard PO, Bay F, Chastel Y. Numerical modelling of crack propagation: automatic remeshing and comparison of different criteria. Comput Methods Appl Mech Eng. 2003;192:3887–908.

[30] Dündar H, Ayhan AO. Three-dimensional fracture and fatigue crack propagation analysis in structures with multiple cracks. Comput Struct. 2015;158:259–73.

[31] Ayhan AO. Simulation of three-dimensional fatigue crack propagation using enriched finite elements. Comput Struct. 2011;89:801–12.

[32] Varfolomeev I, Burdack M, Moroz S, Siegele D, Kadau K. Fatigue crack growth rates and paths in two planar specimens under mixed mode loading. Int J Fatigue. 2014;58:12–9.

[33] Liu G, Zhou D, Guo J, Bao Y, Han Z, Lu J. Numerical simulation of fatigue crack propagation interacting with micro-defects using multiscale XFEM. Int J Fatigue. 2018;109:70–82.

[34] Paris PC, Gomez MP, Anderson WE. A rational analytic theory of fatigue. Trend Eng. 1961;13:9–14.

[35] Paris PC, Erdogan FA. Critical analysis of crack propagation laws. J Basic Eng. 1963;85:528–34.

[36] Elber W. The significance of fatigue crack closure. ASTM STP. Damage tolerance in aircraft structures; 1971.

[37] Newman JR. Prediction of fatigue crack growth under variable-amplitude and spectrum loading using a closure model. Design of fatigue and fracture resistant structures. America: ASTM International; 1982.

[38] Walker K. The effect of stress ratio during crack propagation and fatigue for 2024-T3 and 7075-T6 aluminum; 1970.

[39] Alegre JM, Cuesta II. Some aspects about the crack growth FEM simulations under mixed-mode loading. Int J Fatigue. 2010;32:1090–5.

[40] Erdogan F, Gupta GD, Cook T. Numerical solution of singular integral equations. Methods of analysis and solutions of crack problems. Springer; 1973. p. 368–425.

[41] Kaya AC, Erdogan F. On the solution of integral equations with strongly singular kernels. Q Appl Math. 1987;XLV:105–22.

[42] Mi Y, Aliabadi MH. Three-dimensional crack growth simulation using BEM. Comput Struct. 1994;52:871–8.

[43] Mi Y. Three-dimensional analysis of crack growth. Southampton: Computational Mechanics Publications; 1996.

[44] Hosseini-Toudeshky H, Mohammadi B. Mixed-mode numerical and experimental fatigue crack growth analyses of thick aluminium panels repaired with composite patches. Compos Struct. 2009;91:1–8.

[45] Lucht T. Finite element analysis of three dimensional crack growth by the use of a boundary element sub model. Eng Fract Mech. 2009;76:2148–62.

[46] Roux-Langlois C, Gravouil A, Baietto MC, Réthoré J, Mathieu F, Hild F, et al. DIC identification and X-FEM simulation of fatigue crack growth based on the Williams' series. Int J Solids Struct. 2015;53:38–47.

[47] Mróz KP, Mróz Z. On crack path evolution rules. Eng Fract Mech. 2010;77:1781–807.

[48] Larisa S, Pavel R, Pavel L. A photoelastic study for multiparametric analysis of the near crack tip stress field under mixed mode loading. Procedia Struct Integr. 2016;2:1797–804.

[49] Malíková L, Veselý V, Seitl S. Crack propagation direction in a mixed mode geometry estimated via multi-parameter fracture criteria. Int J Fatigue. 2016;89:99–107.

[50] Smith DJ, Ayatollahi MR, Pavier MJ. The role of T- stress in brittle fracture for linear elastic materials under mixed-mode loading. Fatigue Fract Eng Mater Struct. 2001;24:137–50.

[51] Gupta M, Alderliesten RC, Benedictus R. A review of T-stress and its effects in fracture mechanics. Eng Fract Mech. 2015;134:218–41.

[52] Miranda A, Meggiolaro M, Castro J, Martha L, Bittencourt T. Fatigue life and crack path predictions in generic 2D structural components. Eng Fract Mech. 2003;70:1259–79.

[53] Chudnovsky A, Chaoui K, Moet A. Curvilinear crack layer propagation. J Mater Sci Lett. 1987;6:1033–8.